PHYSICAL REVIEW A VOLUME 41, NUMBER 5 1 MARCH 1990

Laser spectroscopic observation and large-scale configuration-interaction calculation of doubly excited *msns* $^1S^e$ states of Ca atoms

Norio Morita and Toshifumi Suzuki*
Institute for Molecular Science, Myodaiji, Okazaki 444, Japan

(Received 20 September 1989)

With multistep laser excitation via 4*sn's* Rydberg states, doubly excited *msns* $^1S^e$ states ($m=6$, $9\le n\le 20$; $m=7$, $9\le n\le 20$; $m=10$, $10\le n\le 20$ except $n=11$) of Ca atoms have been observed, and their energy levels have been obtained. The large-scale configuration-interaction calculation for Ca atoms has also been executed using a discrete two-electron basis set, in which a frozen Ca^{2+} core is assumed and the total number of the bases is 1714. The calculated energy levels are in good agreement with the observed ones, including those of the 8*sns* and 9*sns* states observed in our previous studies [Phys. Rev. A **38**, 551 (1988); J. Phys. B **21**, L439 (1988)]. Based on the good agreement, charge-density plots have been drawn for the *nsns* states ($4\le n\le 10$), using the calculated eigenvectors. In all the *nsns* states investigated, a reasonably large part of the charge density has been seen to be localized on the Wannier's potential ridge and to show a fairly strong angular correlation. In lower *nsns* states, the angular-correlation pattern has been found to support the moleculelike picture, although an unusual pattern has been seen in a smaller radial region. In higher states, two types of unusual angular correlation have been seen. In particular, one of them is suggestive of a bent structure of the charge-density distribution, in spite of the zero-angular-momentum states. The cause of this correlation has been discussed from a viewpoint of configuration mixing, although its physical meaning is still unknown.

I. INTRODUCTION

For the past two decades, understanding of correlated electronic motion in doubly excited atoms has greatly been developed mainly through two approximate treatments of the Schrödinger equation: one is the SO(4) group theory[1–3,8] and the other the adiabatic approximation using the hyperspherical coordinate.[4–8] The group-theoretical studies have shown that doubly excited states can be well described by the "doubly excited symmetry basis" (DESB) (Ref. 1) diagonalizing an SO(4) Hamiltonian, which is an approximate form of the electron interaction energy. It was also shown that an energy structure described by the DESB of the intrashell states ($n_1=n_2$, where each n_i is a principal quantum number of the electron) is very akin to a rovibronic structure of a linear floppy *X*-*Y*-*X* molecule, where each *X* represents an electron and *Y* the nucleus. Charge-density plots drawn by numerical calculations using the hyperspherical coordinate have strongly supported the correctness of the moleculelike picture in specific doubly excited states including the intrashell states. Similar results have been obtained also by configuration-interaction (CI) calculations.[9] It is also well known that a large part of the charge density in those states lies upon a potential ridge described in the Wannier theory[8,10] for two-electron breakup. Besides, very recently, Iwai and Nakamura[11] have more definitely shown the correctness of the moleculelike picture by the second quantization of the SO(4) Hamiltonian. They have shown that the DESB can be reproduced by rotating and vibrating a symmetry-broken "shape," which is determined by a variational calculation without the symmetry requirement. This shape corresponds to a "molecule," localizing angularly to become a completely linear charge in the limit of a large principal quantum number.

These studies have been developed so far with their main interest focused on a He-like atom consisting of a bare nucleus and of two electrons, i.e., He, H^-, and so on. In the He-like atom, a single-electron state is degenerate, so that, in the language of CI, the mixing among the degenerate states of a given principal quantum number (intrashell mixing) is dominant over intershell mixings even in higher excited states. The studies with the SO(4) group theory is based on this fact and their discussion is restricted within a condition in which each electron has a definite principal quantum number.

On the other hand, in a two-electron atom having an ion core, such as an alkaline-earth atom, the degeneracy of a single-electron state is absent, and a shell structure is significantly broken, especially, in lower-angular-momentum states. Therefore, correlated behaviors of two valence electrons can no longer be described by the SO(4) group theory, though some lowest states of alkaline-earth atoms are found[8,12–14] to be moleculelike by inspecting the wave functions. In those lowest states, in spite of the broken degeneracy, a simple configuration-mixing scheme, such as (*nsns* + *npnp*) in a $^1S^e$ state, is dominant because of wider energy separation of the single-electron energy spectrum, so that those states can be described approximately by the DESB-type wave function having a smaller principal quantum number. In higher states, however, such a simple description should break down because of significant intershell mixings.

It is known that a spherical frozen-core model is a good approximation[12,13,15–19] for alkaline-earth atoms except in their ground states. Therefore, the treatment of their doubly excited states may be interpreted as a natural generalization of a purely Coulombic central-field problem into a non-Coulombic central-field problem. There have, however, hardly been analytical theories suitable for such a more general situation, in which the principal quantum number of each electron is not restricted to a definite value. Therefore, there is still much room for these atoms to be studied not only theoretically but also experimentally, including a question of whether a specific regularity alternative to the moleculelike picture does exist.

Under these backgrounds, we have so far been investigating doubly excited states of Ca atoms experimentally. As for experimental observations, higher doubly excited states of alkaline-earth atoms are much easier to observe than those of He-like atoms, because laser spectroscopic techniques can be applied to the former and a detailed observation is possible with a sufficient frequency resolution. Among many doubly excited states, the most interesting is a state in which the two electrons have a common principal quantum number at least in their dominant configurations. This state is expected to be the Wannier-ridge-type[8,20–22] state and to have the strongest electron correlation. Although a number of doubly excited states of alkaline-earth atoms have been observed with a laser spectroscopic method mainly using the isolated-core excitation scheme,[23–33] it has been quite difficult to observe a state in which a difference between the principal quantum numbers of the two electrons is less than 3.[30] In Ca atoms, however, the present authors fortunately observed[31,32] some *msns* $^1S^e$ and *mdns* $^1D^e$ states in which *n* is equal to or differs from *m* by less than 3, though their assignment was only tentative.

After those works we have continued the observation of doubly excited states of Ca atoms. Among the results so far obtained, we concentrate our interest on those of the *msns* $^1S^e$ states in this paper and will show the results of more extended observation than the previous ones. We have also carried out a large-scale CI calculation to compare the calculated results with the experimental data and to examine the correctness of the tentative assignment of the experimental data mentioned above. Configuration-mixed eigenvectors and their eigenvalues have been obtained by straightforward diagonalization of the Hamiltonian composed of a discrete two-electron basis. As a result, we have seen good agreement between the calculated and observed energy levels, and, in particular, the assignment of some pure and near Wannier-ridge-type states has satisfactorily been confirmed. Based on this good agreement, charge density plots of the Wannier-ridge-type states have also been drawn by using the calculated eigenvectors. The plots have been found to show definitely different correlation patterns from those of a He-like atom, especially in the angular correlation. Though the physical meaning of the unusual angular correlation is still unknown, its direct cause will be detailed from a viewpoint of the configuration mixing.

II. EXPERIMENTAL PROCEDURE AND RESULTS

The excitation method for the doubly excited states is the same as that described in the previous papers,[31,32] and is called the "isolated-core excitation" method, which is developed by Cooke and co-workers.[23,24] In brief, one of the valence electrons of a Ca atom is first excited to an *n's* Rydberg state via the 4*p* state by two pulsed blue lasers with a 7-ns pulse width, and after 20 ns another valence electron left in the 4*s* state is excited to an *ms* state through two-photon absorption of a third uv laser. The role of the first process, which is completely separated from the second one, is only a preparation of the initial state for the second one. The second process is an excitation of the Ca^+ core when it is seen by the Rydberg electron, and this process has little influence on the Rydberg electron as long as the Rydberg state is much higher than the final *ms* state of the core electron. This description is called the "isolated-core approximation." It is an origin of the name of this excitation method, and a spectrum observed with this method is called the "core-excitation spectrum." Doubly excited states thus created quickly autoionize into some excited states of Ca^+ ions, which are further photoionized into Ca^{2+}. We detect these Ca^{2+} ions through a time-of-flight mass spectrometer and measure their ion current as a function of the uv laser wavelength.

We have so far observed the spectra of the doubly excited *msns* states in which $m = 6-10$. The observed spectra are shown in Fig. 1, in which only the spectra of the 6*sns*, 7*sns*, and 10*sns* states are presented because those of the 8*sns* and 9*sns* states have already been published.[31,32] Each of Figs. 1(a), 1(b), and 1(c) shows a group of two-photon core-excitation spectra observed in a common wavelength region, and each trace shows a spectrum obtained when the initial state denoted at the left side of each trace is populated by the blue lasers. A sharp feature, denoted by *A*, *B*, and *C* at the top of each spectrum group, is seen in every trace of each group. Those features *A*, *B*, and *C* are the $4s \rightarrow 6s$, $4s \rightarrow 7s$, and $4s \rightarrow 10s$ two-photon resonance lines of Ca^+, respectively. These resonance lines play important roles in assigning doubly excited states observed. Similar sharp features denoted by *D*, *E*, *F*, *G*, and *H*, being Ca^+ resonances with initial states other than the 4*s* state, have no more meaning than frequency markers. Note that the Ca^+ resonances appear because many Ca^+ ions are produced as byproducts of the laser excitation. Broader features in the vicinity of or overlapped with each $4s \rightarrow ms$ resonance of Ca^+ are the $4sn's \rightarrow msns$ core-excitation resonances of neutral calcium.

The spectra shown in Fig. 1 are all obtained using a linearly polarized uv laser. Therefore, they contain some resonances of the *mdns* $^1D^e$ states. We have distinguished the $^1S^e$ states from the $^1D^e$ states through a complementary observation using a circularly polarized uv laser, with which a resonance of a $^1S^e$ state should disappear while that of a $^1D^e$ state should remain. The resonances of the $^1D^e$ states thus confirmed are denoted by *x* in Fig. 1.

Concerning the core-excitation spectrum, detailed ex-

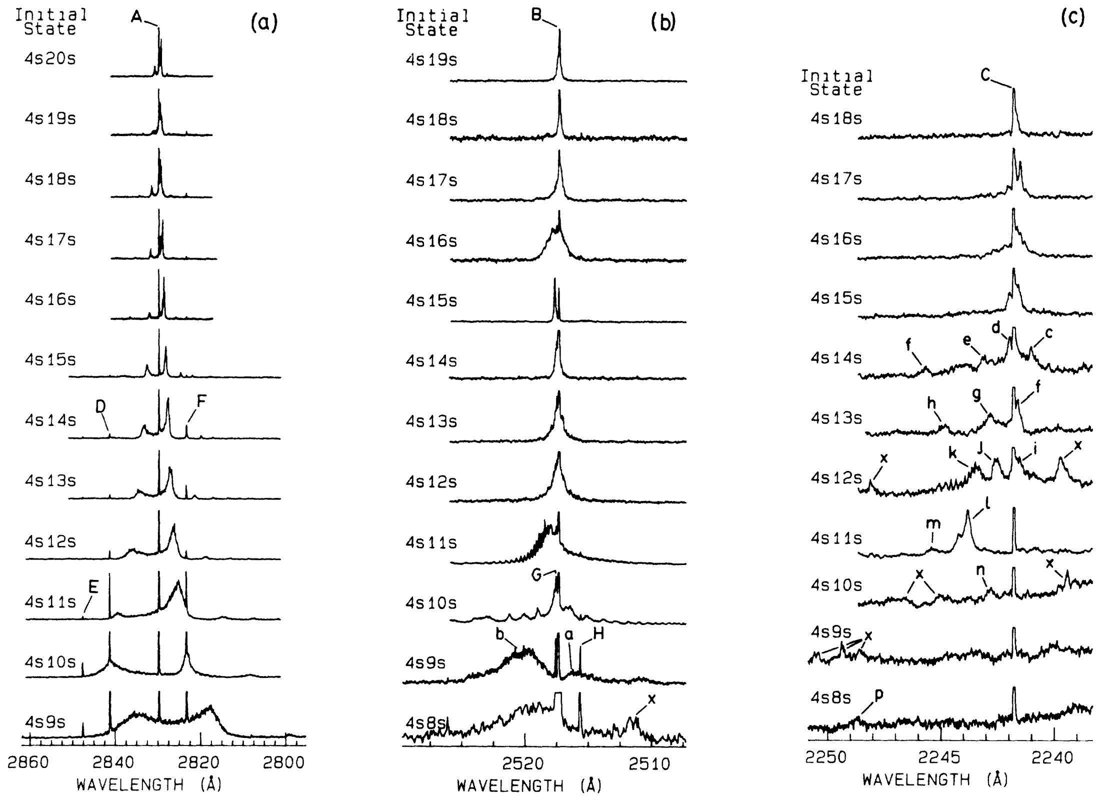

FIG. 1. Two-photon excitation spectra observed in the wavelength region around (a) $4s\rightarrow 6s$, (b) $4s\rightarrow 7s$, and (c) $4s\rightarrow 10s$ two-photon resonances of Ca^+: the abscissa is the uv laser wavelength and the ordinate is Ca^{2+} ion current resulting from the laser excitation. Each trace is obtained when the initial $4sn's$ state denoted at the left side of each trace is populated. The narrow features denoted by A, B, and C are the $4s\rightarrow 6s$, $4s\rightarrow 7s$, and $4s\rightarrow 10s$ resonances of Ca^+, respectively, and broader features around those $4s\rightarrow ms$ Ca^+ resonances are the $4sn's\rightarrow msns$ core-excitation resonances of neutral Ca. Other narrow features denoted by D–H, being also Ca^+ resonances, have no importance in the present study. Small letters a–p, denoting specific broader resonances of the doubly excited states, are written for the sake of the correspondence with the energy levels presented in Table I. Features denoted by x are not resonances of $msns$ states but of $mdns$ states.

planations have been made by many authors.[24,28,30,33] In brief, as long as the isolated-core approximation holds good, the spectral intensity is proportional to

$$I=|\mu^{\mathrm{core}}|^2\frac{4\nu'\nu}{(\nu'+\nu)^2}\left[\frac{\sin[\pi(\nu'-\nu)]}{\pi(\nu'-\nu)}\right]^2|A(\nu)|^2\,, \qquad (1)$$

where μ^{core} is the two-photon transition matrix element of the $4s\rightarrow ms$ transition of the Ca^+ core, ν' and ν are effective quantum numbers of the Rydberg electron in the initial and final states, respectively, and $A(\nu)$ is a spectral density function of the final state. The energies of the initial and final states are given as

$$\begin{aligned}E(4sn's)&=E(\mathrm{Ca}^+{:}4s)-R/\nu'^2\\&=E(\mathrm{Ca}^+{:}4s)-R/(n'-\delta')^2\,,\\E(msns)&=E(\mathrm{Ca}^+{:}ms)-R/\nu^2\\&=(\mathrm{Ca}^+{:}ms)-R/(n-\delta)^2\,,\end{aligned}$$

respectively, where $E(\mathrm{Ca}^+{:}ns)$ is the energy of the ns state of Ca^+, δ' and δ are quantum defects of the initial and final states, respectively, and R is the Rydberg constant. Then, the uv laser wavelength is expressed as

$$\lambda_{\mathrm{uv}}=2hc/[E(\mathrm{Ca}^+{:}ms)-E(\mathrm{Ca}^+{:}4s)-R/\nu^2+R/\nu'^2]\,. \qquad (2)$$

As can be seen in Eqs. (1) and (2), strong resonances of the $4sn's\rightarrow msns$ core excitation appear only in the vicinity of the $4s\rightarrow ms$ resonance of Ca^+, because this Ca^+ resonance appears just at a wavelength in which $\nu=\nu'$. This formula holds quite good in the traces observed with higher initial states, as is seen in Fig. 1. In fact, some spectra can be just fitted to Eq. (1), as shown in the previous paper.[31]

A frequency shift of the core-excitation resonance from the Ca^+ resonance reflects a fraction part of a difference between δ' and δ, and we can determine the fraction part from the observed spectra. In Figs. 1(b) and 1(c), each core-excitation resonance almost overlaps with the corresponding $4s\rightarrow ms$ resonance of Ca^+, and this means that δ differs from δ' approximately by an integer. For each doubly excited $msns$ state with m fixed, the fraction part of δ is found to be roughly constant at least over the states observed with higher initial states. An integer part of δ cannot be obtained through this treatment and thus the principal quantum number n of the final state is undetermined. A quantum defect primarily reflects a size of the Ca^+ core penetrated by the Rydberg electron, so that it should become larger with the Ca^+ core size increased, that is, with m increased. As was tried by Bloomfield *et al.*[27] for Ba atoms, we can choose the integer part of δ so that δ increases linearly depending on m. The δ value averaged over higher doubly excited states is plotted as a function of m in Fig. 2. The slope of the increase is 0.32, which is very close to the value obtained for Ba atoms.[27,28]

The linear dependence of the quantum defect on m, in fact, can be predicted by a simple theoretical calculation, in which a wave function of the inner electron is calculated assuming a frozen Ca^{2+} core with an empirical core-polarization effect incorporated and then the energy of the outer electron is calculated under an overall potential produced by both the Ca^{2+} core and the inner electron. The frozen core used here is the same as that used in the CI calculation in Sec. III. For each m fixed, the quantum defect thus calculated for the *msns* states is almost constant at least over $n \geq 14$. The value averaged over $n = 14-18$ is plotted with triangles in Fig. 2, and it definitely shows a linear dependence on m. The slope is, however, 0.227, which is considerably smaller than the experimental value. While the agreement between the theoretical and experimental values is quite good for $m = 4$, the mutual deviation becomes larger with m increased. This fact suggests that, even in the $m \ll n$ states, the electron correlation is not negligible when both electrons are highly excited. In spite of this disagreement, our choice of the integer parts of the quantum defects is considered reasonable, because the calculated values are primarily correct enough to show an essential tendency and it is quite unrealistic to shift each experimental δ value by a nonzero integer from the value shown in Fig. 2. Moreover, as shown in Ref. 36, the quantum defect values determined by our choice of the integer values are in fairly good agreement with those derived from a one-electron Rydberg formula incorporating the electron correlation effect. This fact also supports the correctness of the choice.

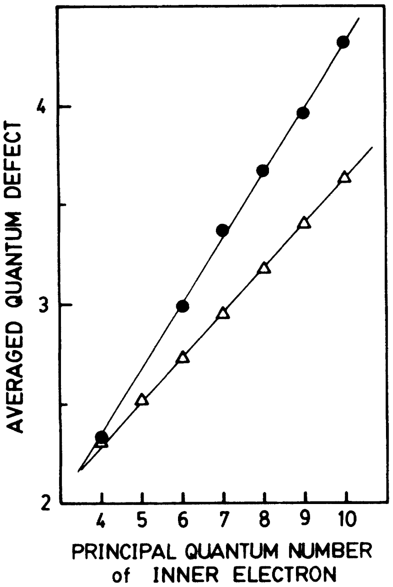

FIG. 2. Observed and calculated quantum defects as a function of the principal quantum number of the inner electron: each quantum defect is averaged over higher Rydberg states. Observed data are marked by solid circles and calculated ones by triangles. Each straight line is fitted to the respective data group.

By the δ values thus determined, we can assign the principal quantum number n of the final doubly excited state. In Fig. 1(a), the final state of each resonance at a shorter wavelength side of the $4s \rightarrow 6s$ ionic line is the $6s(n'+1)s$ state, and that of each resonance at a longer wavelength side the $6sn's$ state, where n' is a principal quantum number of the initial Rydberg state. In Fig. 1(b), the final state of each resonance overlapped with the $4s \rightarrow 7s$ ionic line is the $7s(n'+1)s$ state. Similarly in Fig. 1(c), that of each resonance almost overlapped with the $4s \rightarrow 10s$ line is the $10s(n'+2)s$ state, though the resonances are significantly split into many peaks, especially in lower traces. This splitting is due to an interference of the wave function with other doubly excited Rydberg series, and a similar feature is also seen in lower traces in Fig. 1(b). The split features in the $7s11s$ and $7s12s$ states are caused by the interference with the $5fnf$ and $5gng$ Rydberg series, and those seen in the states from $10s13s$ to $10s16s$ are due to the interference with the $9dnd$ and $8lnl$ ($l = 3-7$) series. Moreover, an additional interference pattern with the $9pnp$ series is overlapped with the $10s13s$ and $10s14s$ states.

In exciting the $n \approx m$ states, the isolated-core approximation must break down, so that Eq. (1) does not hold. However, the excitation scheme itself, in which the electrons are excited one by one, is considered still applicable, and those states are expected to be observed as long as a cross section of the relevant transition is large enough. In fact, we have successfully observed the *7sns* states in which n is down to 9. Furthermore, we have also observed the $10s12s$ and $10s10s$ states, which are denoted by n and p in Fig. 1(c), respectively, though the $10s11s$ has not been observed. Those resonances have been confirmed not to be due to any transitions either from the $4s4s$ ground state nor from the $4s4p$ intermediate state of the laser excitation. Moreover, by using a circularly polarized laser, the final states of those resonances have been confirmed to be the $^1S^e$ states. The detection sensitivity in this case is limited by the background Ca^{2+} current caused by various resonant or nonresonant photoionization processes. In a wavelength region around 2235 Å, in particular, there is a very broad resonance of a two-photon transition starting from the ground state. It considerably diminishes the sensitivity in the observation of the *10sns* series. For the *6sns* series, we have not been able to observe any state below the $6s9s$ state because of the limitation of the present detection scheme. That is all the 6*sns* states lying below the 6*s*9*s* state are so low in energy that any Ca^+ state produced by the autoionization of those 6*sns* states cannot reach the double ionization limit by absorbing a uv photon.

The energy levels of all doubly excited states thus observed are listed in Table I. For the 6*sns* and 7*sns* states, the energy has been obtained in most cases by fitting Eq. (1) to each trace, assuming the spectral density function calculated by the two-channel quantum-defect theory,[33,34] and assuming also that the quantum defect and the autoionization width are both linearly dependent on energy within the wavelength region of each trace. An envelope form has been fitted for a state showing a slight interference pattern, such as the 7*s*12*s* state. For

TABLE I. Observed and calculated energy levels of the doubly excited *msns* $^1S^e$ states of Ca. For the states corresponding to more than one calculated eigenstate, all the calculated levels are written: Lower levels are denoted by only the last digits different from those of the highest one. NO, not observed in the experiment; ND, not distinguished in the results of the CI calculation.

n	*E*(obs) (a.u.)	*E*(calc) (a.u.)
	6*sns*	
20	−0.115 99(3)	−0.116 04
19	−0.116 24(1)	−0.116 20
18	−0.116 48(1)	−0.116 37
17	−0.116 79(1)	−0.116 67
16	−0.117 18(1)	−0.117 06
15	−0.117 68(1)	−0.117 54
14	−0.118 34(1)	−0.118 18
13	−0.119 19(1)	−0.118 96
12	−0.120 37(3)	−0.120 28
11	−0.122 01(4)	−0.121 73
10	−0.124 07(8)	−0.123 98
9	−0.126 14(11)	−0.128 44
8	NO	−0.133 36
7	NO	−0.140 89,751
6	NO	−0.174 82
	7*sns*	
20	−0.076 09(1)	−0.076 01
19	−0.076 32(1)	−0.076 20
18	−0.076 60(1)	−0.076 46,57,78
17	−0.077 00(3)	−0.077 07
16	−0.077 45(1)	−0.077 41
15	−0.077 97(1)	−0.077 85
14	−0.078 69(2)	−0.078 38,76
13	−0.079 64(2)	−0.079 57
12	−0.081 05(5)	−0.081 12,6
11	−0.082 84(4)	−0.082 59
10	−0.085 37(5)[a]	−0.085 29
	−0.085 96(10)[b]	−0.086 08
9	−0.090 14(11)	−0.090 21
8	NO	−0.097 77
7	NO	−0.113 02
	8*sns*	
20	−0.054 05(1)	−0.054 02
19	−0.054 30(1)	−0.054 26
18	−0.054 60(1)	−0.054 48,58,66
17	−0.054 98(1)	−0.054 94,7
16	−0.055 44(1)	−0.055 43
15	−0.056 09(1)	−0.056 05
14	−0.056 86(1)	−0.056 82
13	−0.057 93(1)	−0.057 90,8
12	−0.059 40(2)	−0.059 36,43
11	−0.061 71(3)	−0.061 64
10	−0.065 00(8)	−0.064 59,87
9	−0.070 18(14)	−0.069 43,7035
8	NO	−0.079 77,8006
	9*sns*	
20	−0.040 58(1)	−0.040 57
19	−0.040 85(1)	−0.040 81
18	−0.041 20(1)	−0.041 07,27
17	−0.041 61(1)	−0.041 59
16	−0.042 10(1)	−0.042 08
15	−0.042 74(1)	−0.042 67
14	−0.043 64(2)	−0.043 58
13	−0.044 82(5)	−0.044 87,99
12	−0.046 58(3)	−0.046 39
11	−0.049 25(6)	−0.049 05,29,36,51
10	−0.055 66(5)	ND
9	−0.060 36(4)	−0.060 24
	10*sns*	
20	−0.031 81(2)	−0.031 79,80
19	−0.032 08(2)	−0.032 06
18	−0.032 44(2)	−0.032 29,48
17	−0.032 89(2)	−0.032 90,1
16	−0.033 32(1)[c]	−0.033 38
	−0.033 46(3)[d]	−0.033 43
	−0.033 70(1)[e]	−0.033 84
15	−0.034 15(1)[f]	−0.034 12
	−0.034 37(1)[g]	−0.034 28,44
	−0.034 73(3)[h]	−0.034 79
14	−0.035 10(3)[i]	−0.035 07,11
	−0.035 27(1)[j]	−0.035 27
	−0.035 43(2)[k]	−0.035 51
13	−0.036 82(1)[l]	−0.036 72
	−0.037 11(3)[m]	−0.036 99
12	−0.038 48(2)[n]	−0.038 14,900
11	NO	−0.04127
10	−0.046 61(4)[p]	−0.046 12,39

[a–p]Energy level obtained from a specific resonance denoted by the same small letter in Fig. 1.

the 6*s*18*s* and 7*s*11*s* states as well as the highest four 10*sns* states, the fitting has not been executed because of their severely split feature or of their heavy overlapping with the ion resonances, but the wavelength of only the highest peak has been directly measured. Similarly, for all the 10*sns* states below 10*s*17*s*, because of their strongly split form and of the varying background level, the fitting has not been executed, but the wavelength of each peak has been directly measured.

III. CI CALCULATION

The present CI calculation is executed using a discrete two-electron basis. Configuration-mixed wave functions and their energy levels are obtained by straightforward diagonalization of a Hamiltonian matrix composed of the two-electron basis.

Each single-electron wave function of the basis is calculated under an *e*-Ca^{2+} interaction potential and under the usual boundary condition (zero amplitude at $r \rightarrow \infty$). A good description of the *e*-Ca^{2+} interaction is very important in order to obtain a proper two-electron basis. We use the same *e*-Ca^{2+} interaction potential as that used by Kim and Greene[19] in their *R*-matrix calculation. The potential consists of a screening term and of an empirical core-polarization term

$$v_l(r)=v_l^{\mathrm{HS}}(r)-\frac{\alpha_{\mathrm{cp}}}{2r^4}\{1-\exp[-(r/r_{cl})^6]\} \ . \qquad (3)$$

The screening term $v_l^{\mathrm{HS}}(r)$ is determined by executing a Hartree-Slater-type calculation of Ca^+. The core polarization α_{cp} and the *l*-dependent cutoff radius r_{cl} is determined to obtain optimum agreement with the known spectrum of Ca^+. Because of a wider energy range of the present CI calculation than that in Ref. 19, the $v_l^{\mathrm{HS}}(r)$ term as well as r_{cl} are determined to be dependent on l up to 4, and the core-polarization parameters are optimized by fitting the lowest four states for each l. The final values obtained are $\alpha_{\mathrm{cp}}=6.76$, $r_{c0}=2.16$, $r_{c1}=2.81$, $r_{c2}=1.832$, $r_{c3}=5.35$, and for $l \geq 4$, $r_{cl}=8.64$. The last two values indicate that the core-polarization effect is almost negligible for states with $l \geq 3$. For the sake of a later estimation of the accuracy of the CI calculation, the calculated energy levels of Ca^+ and their residual errors are listed together with the observed levels in Table II.

Each two-electron base is an antisymmetric *LS*-coupled $mlnl\ {}^1S^e$ base, in which the quantum numbers, l, m, and n are chosen as $0 \leq l \leq l_0$, $4 \leq m \leq m_0$ for $l=0$ and 1, $3 \leq m \leq m_0-1$ for $l=2$, $l+1 \leq m \leq m_0-2$ for $l \geq 3$, and $m \leq n \leq n_0$. The maximum values l_0, m_0, and n_0 are determined to obtain a good convergence of the eigenvalues corresponding to the states observed experimentally. When l_0 is varied from 9 to 11 with $m_0=17$ and $n_0=24$ fixed, only a negligible change is seen in the eigenvalues. Similarly, when m_0 is varied from 12 to 17 with $l_0=9$ and $n_0=24$ fixed, the change is also negligible. Finally, when n_0 is varied up to 38 with l_0 and m_0 fixed to 9 and 12, respectively, a reasonable convergence is seen as n_0 approaches 38. Thus, all results below are obtained using the basis set in which $l_0=9$, $m_0=12$, $n_0=38$, and the number of the bases is 1714.

The accuracy of numerical integrals in the calculation of the Hamiltonian-matrix elements is so satisfactory that

TABLE II. Calculated and observed energy levels of Ca^+ and their mutual differences.

States	*E*(calc) (a.u.)	*E*(obs) (a.u.)	*E*(calc)−*E*(obs) (a.u.)	States	*E*(calc) (a.u.)	*E*(obs) (a.u.)	*E*(calc)−*E*(obs) (a.u.)
4*s*	−0.436 37	−0.436 28	−0.000 08	9*d*	−0.028 65	−0.028 54	−0.000 11
5*s*	−0.198 38	−0.198 59	0.000 21	10*d*	−0.022 85	−0.022 77	−0.000 08
6*s*	−0.114 12	−0.114 25	0.000 13				
7*s*	−0.074 21	−0.074 29	0.000 07	4*f*	−0.126 27	−0.126 19	−0.000 08
8*s*	−0.052 13	−0.052 18	0.000 04	5*f*	−0.080 65	−0.080 73	0.000 08
9*s*	−0.038 63	−0.038 66	0.000 03	6*f*	−0.055 94	−0.056 02	0.000 07
10*s*	−0.029 77	−0.029 79	0.000 02	7*f*	−0.041 07	−0.041 12	0.000 05
				8*f*	−0.031 42	−0.031 46	0.000 04
4*p*	−0.320 97	−0.320 82	−0.000 14	9*f*	−0.024 81	−0.024 84	0.000 03
5*p*	−0.159 92	−0.160 23	0.000 31	10*f*	−0.020 09	−0.020 11	0.000 02
6*p*	−0.096 60	−0.096 79	0.000 19				
7*p*	−0.064 77	−0.064 89	0.000 12	5*g*	−0.080 15	−0.080 13	−0.000 02
8*p*	−0.046 47			6*g*	−0.055 63	−0.055 64	0.000 01
9*p*	−0.034 97			7*g*	−0.040 86	−0.040 87	0.000 02
10*p*	−0.027 27			8*g*	−0.031 28	−0.031 29	0.000 01
				9*g*	−0.024 71	−0.024 72	0.000 01
3*d*	−0.373 65	−0.373 92	0.000 27	10*g*	−0.020 01		
4*d*	−0.178 57	−0.177 25	−0.001 32	6*h*	−0.055 61		
5*d*	−0.105 61	−0.104 91	−0.000 70	7*h*	−0.040 85		
6*d*	−0.069 78	−0.069 38	−0.000 40	8*h*	−0.031 27	−0.031 26	−0.000 01
7*d*	−0.049 53	−0.049 28	−0.000 25	9*h*	−0.024 71		
8*d*	−0.036 97	−0.036 81	−0.000 16	10*h*	−0.020 01	−0.020 01	−0.000 00

an overlap integral of any two wave functions having a common l is typically as small as an order of 10^{-12}. The accuracy of the diagonalization is examined by comparing every vector element between both sides of the eigenvalue equation after each eigenvalue and its eigenvector are substituted into the equation. As a result, it is found that both sides of the equation agrees with each other typically within a relative difference of 10^{-8}.

It is generally difficult to assign the eigenstates obtained from the CI calculation. High-lying doubly excited states in particular are very difficult to assign, because in the language of the multichannel quantum-defect theory,[34] many channels interact with each other. Highly excited Rydberg states, however, can easily be distinguished by inspecting their eigenvectors. In those states, the independent-electron picture holds good, so that the configuration-mixed eigenvector is expected to have a dominant contribution from the *msns* bases having a constant m ($m \ll n$). In fact, a calculated eigenstate, which is finally assigned to the $6s20s$ state, has a more than 83% contribution from the $6sns$ bases. This characteristic becomes less remarkable in a Rydberg state in which the inner electron is more highly excited. For example, an eigenstate, which is finally assigned to the $9s20s$ state, has only a 65% contribution from the $9sns$ bases. The residual 35% part occupied by other *mlnl* bases partly contributes to both radial and angular correlations and results in lowering the energy. This tendency is consistent with that shown in Fig. 2, in which, as the inner electron is more highly excited, the observed quantum defects tend to become larger than those calculated assuming the complete independent-electron picture.

Each highly excited Rydberg state observed is assigned to a single calculated eigenstate in most cases, while in some cases a group of a few eigenstates corresponds to an observed state. In both cases, the calculated energy levels of highly excited Rydberg states are in good agreement with the observed ones. Furthermore, energy spacings of the calculated levels also agree well with those observed. We can thus continue easily to assign the calculated eigenstates to the observed states from a higher Rydberg state down to nearly the lowest state of the Rydberg series. In fact, the easiness in this assignment holds approximately down to a state in which a difference between the principal quantum numbers of the two electrons is 3. Below this state, the mixing among many bases becomes so remarkable that it is more difficult to distinguish the objective eigenstate. It is interesting to note that the difficulty in the experimental observation also occurs below this state,[30] as was mentioned in Sec. I. This correspondence might mean the difficulty of exciting a highly correlated state from a less correlated $4sns$ Rydberg state, as is pointed out by Rau,[35] because a high degree of configuration mixing generally corresponds to a strong correlation. Those, however, which mix into the objective eigenstate and obscure the assignment are dominantly Rydberg-type ($mlnl$:$m \ll n$) bases of lower-lying Rydberg series. The mixing of a number of those Rydberg-type bases smears the objective state. This means that the difficulty in the observation may result rather from this smearing than from the electron correlation. In spite of this difficulty, it is still possible to assign these lower states with a reasonable certainty. For the lowest state of a Rydberg series, the correctness of the assignment is also confirmed by the fact that its charge-density distribution is of the Wannier-ridge-type, as will be shown in Sec. IV.

The calculated energy levels thus assigned are listed in Table I. As is seen in Table I, the difference from each observed energy level is roughly equal to or less than 1×10^{-4} a.u. in higher states of each Rydberg series, and is about 2×10^{-4} a.u. in lower states except in a few particular states. Considering the accuracy of the calculated Ca^{+} energy levels, this agreement is quite satisfactory. The agreement is generally better in higher Rydberg series than in lower series. This directly reflects the fact that the accuracy of the Ca^{+} energy levels is better in higher states. It is, in fact, found that in many eigenstates the calculated energy levels tend to be improved when they are shifted by a value of the error of a Ca^{+} energy level corresponding to the ionization limit of each Rydberg series.

The worst agreement is seen in the $6s9s$ state. As is seen in the lowest trace of Fig. 1(a), this resonance is considerably shifted toward higher energy than expected if the usual Rydberg formula $E=-1/[2(n-\delta)^2]$ with a constant quantum defect δ were assumed. Although this unusual shift is probably due to an interaction with other channels, it is not reproduced in the calculated results. This disagreement is also likely to result from worse accuracy of lower energy levels of Ca^{+}, in particular, in the *md* states.

One of the purposes of the present calculation is to confirm the tentative assignment of the observed states in which a difference of two electrons' principal quantum numbers is less than 3, because those states have never been observed clearly in any alkaline-earth atom before our observation. As seen in Table I, though differences between the calculated and observed energy levels tend to be somewhat larger in those states than in higher Rydberg states, the differences are generally small enough to conclude that the assignment is satisfactorily confirmed in most of those states. In the state for which more than one calculated levels are presented in Table I, at least one of those values is close to the observed energy. The other eigenstates are likely to have been missed in the observation because of the low intensity of their resonances. In the $9s11s$ state, which is shown in Ref. 31, its resonance observed is remarkably split into many peaks, and this split feature is well reproduced by the calculated result through the presence of many calculated eigenstates corresponding to this state. The most queer is the $9s10s$ state. As is shown in Ref. 31, the observed resonance is unusually shifted toward lower energy, and we cannot assign this resonance to any calculated eigenstate. Far from that, we cannot distinguish any eigenstate corresponding to the $9s10s$ state. In the energy region where the $9s10s$ eigenstate is expected to exist, the $9sns$ bases are very dispersively distributed over many eigenstates, and these bases make only a small contribution to any eigenstate around there. In this region, the $8sns$, $8pnp$, $7dnd$, and $6lnl$ ($l=3$, 4, and 5) Rydberg-type bases are prevailing and smearing the 9s10s eigenstate. Thus, the assignment of the observed resonance still remains undetermined.

As for the 9s9s state, good agreement is seen between the calculated and observed energy levels. The observed resonance of this state is very strong for a Wannier-ridge-type state, while other states of this type are not observed or very weak. On the other hand, for an unknown reason, the calculated eigenstate assigned to the 9s9s state has a considerably large contribution (about 20%) from the 9s9s base, while any other Wannier-ridge-type eigenstate has only a small contribution from the corresponding *msms* base. This coincidence between the intensity of the observed resonance and the characteristics of the calculated eigenvector is similar to that described before. The large contribution from the 9s9s base might result in the observed large transition cross section from the initial 4s8s state being less correlated. This, however, does not necessarily mean a weaker electron correlation in this state than in other Wannier-ridge-type states, as will be shown in the charge-density plot.

As for the 10s10s state, there are two eigenstates corresponding to this state. The one with an energy of −0.046 39 is the same eigenstate as that assigned to the 9s12s state. In fact, the observed energy of the 10s10s state is equal to that of the 9s12s state within the experimental error. However, the resonance assigned to the 10s10s state, which is shown in the lowest trace in Fig. 1(c), is not the one resulting from the 4s→9s core-excitation process, because no neighboring resonances, such as the 9s11s and 9s13s states, are seen in the same trace. It is, therefore, more reasonable to consider that this resonance is due to the 4s→10s core excitation. It is confirmed by the charge-density plot that this eigenstate is Wannier-ridge-type, though it has also a characteristic of the 9s12s state. We note that the other eigenstate has, somewhat more clearly, the characteristic of the Wannier-ridge-type state. In any case, a difference between these two calculated levels is not so large, and they are both in reasonable agreement with the observed energy level.

For only the *nsns* states, Aymar[36] has very recently executed a moderate-size CI calculation using wave functions with their amplitudes forced to vanish at $r=100$ a.u. Our calculated energy levels of the *nsns* states approximately equal to those calculated in Ref. 36. There are, however, still definite differences between both results; for example, our calculated energy level of the 9s9s state (−0.060 24 a.u.) is different by roughly 0.001 a.u. from that in Ref. 36 (−0.0611 a.u.). Though a difference between the above two calculated levels might be too small to be appreciated, it would be important if it results from a difference in the boundary condition of the wave functions used. Before executing the present calculation, however, we have also executed another CI calculation using wave functions with a boundary condition similar to that in Ref. 36, that is, with their amplitudes forced to vanish at $r=130$ a.u., and using 1340 two-electron bases. As a result, for all the *nsns* states, we have obtained almost the same energy values as those of the present calculation. Therefore, we can conclude that the difference between the results in Ref. 36 and in the present study is not caused by the difference in the boundary condition. It is possible that a size of the basis set used in Ref. 36, which is much smaller than ours, results in the difference of the energy values.

It is interesting to test the applicability of a two-electron Rydberg formula[20–22] to Ca *nsns* levels. Some different types of the formula have so far been proposed and tested. As for the Ca *nsns* levels, Aymar has shown[36] that Wang's formula[37] is good enough to describe the energy levels obtained by the CI calculation. In the present study, we try to test another formula proposed by Rau.[21] The test of this formula has been demonstrated for the *nsnp* $^1P^o$ Wannier-ridge-type states by Kim and Greene.[19] This formula is given as (in a.u.)

$$E=-\frac{4(Z-1/4-\sigma)^2}{(n+3/2-\mu)^2}\ , \tag{4}$$

where Z is the charge of the residual Ca^{2+} ion core, σ is an effective screening parameter, and μ is the quantum defect resulting from specific interactions between the electron pair and the Ca^{2+} core. The principal quantum number n takes on positive integer values. For the sake of direct comparison with the result in Ref. 19, the same representation as theirs is applied to our result; that is, when the energy level is scaled on an effective quantum number ν, Eq. (4) is transformed as

$$\nu=\frac{n+\frac{3}{2}-\mu}{2\sqrt{2}(Z-1/4-\sigma)}\ , \tag{5}$$

so that a linear dependence of ν on n is expected. In fact, the calculated energy levels in Fig. 3 clearly show the linear dependence. The straight line is calculated by Eq. (5) using the same Z dependence of σ as that used in Ref. 19. Note that this Z dependence is the one obtained for an electron pair moving in the field of a point nucleus. The slope of the calculated energy levels is 0.402, and

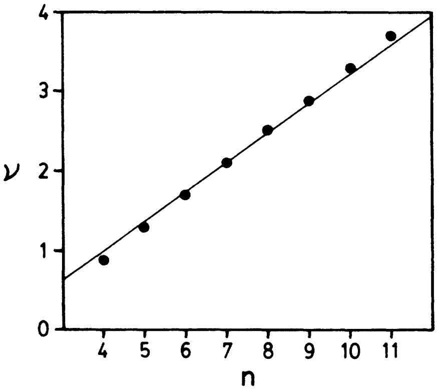

FIG. 3. Effective quantum numbers ν of *nsns* energy levels of Ca. Solid circles denote the results of the CI calculation. The straight line is calculated by the two-electron Rydberg formula [Eq. (5)]: the quantum defect μ is adjusted so that both results agree with each other at $n=7$.

differs from that of the straight line by about 9%. This difference is comparable to that seen in the *nsnp* $^1P^o$ states. The correctness of our calculated energy levels are supported by the experimentally observed results at least for the 9*s*9*s* and 10*s*10*s* states, and there is no question on the 4*s*4*s* state. Therefore, it is reasonable to consider the above difference as a fundamental difference between calcium and helium, such as the nondegeneracy of Ca^+ levels. On the other hand each effective quantum number is uniformly smaller than that of the $^1P^o$ state. This is quite reasonable, considering the usual idea on the quantum defect, that is, for a fixed core, an *s* electron has a larger quantum defect than a *p* electron, because a larger part of an *s* electron is overlapped with the core than a *p* electron.

IV. CHARGE-DENSITY PLOTS

In this section, based on the good agreement between the observed spectra and the results of the CI calculation, charge-density plots of the doubly excited states of Ca are drawn using the calculated eigenfunctions, and behaviors of the electron correlation are investigated. In the present work, we concentrate our interest on the Wannier-ridge-type states because they are expected to show most strongly correlated behaviors.

There may be various choices of independent variables for drawing the plot.[6,8,9,13,14] We use in this work the usual hyperspherical-coordinate variables $\alpha=\tan^{-1}(r_2/r_1)$ and $\theta=\cos^{-1}[\mathbf{r}_1\cdot\mathbf{r}_2/(r_1r_2)]$, though it is not necessarily meaningful to use them in the present case because of the significant breakdown of the adiabatic approximation in Ca. This choice is because it is important and interesting to compare the present results directly with a number of α-θ plots so far drawn for He-like atoms. We also draw another type of charge-density plots as a function of r_1 and r_2 in order to compensate information lost in the α-θ plots.

These two expressions $P(\alpha,\theta;R)$ and $Q(r_1,r_2)$ of charge density are defined as follows:

$$P(\alpha,\theta;R)=\rho(R\cos\alpha,R\sin\alpha,\theta)\ , \tag{6}$$

$$Q(r_1,r_2)=\int_0^\pi \rho(r_1,r_2,\theta)\sin\theta\, d\theta\ , \tag{7}$$

where

$$\rho(r_1,r_2,\theta)=\frac{8\pi^2r_1^2r_2^2}{2L+1}\sum_{M=-L}^{L}|\Psi_{\mathrm{LM}}|^2\ , \tag{8}$$

$R=(r_1^2+r_2^2)^{1/2}$ is a hyperradius, and Ψ_{LM} is an eigenfunction composed of the calculated CI coefficients and of the antisymmetric *LS*-coupled two-electron basis functions used in the CI calculation. Note that the charge densities *P* and *Q* satisfy

$$1=\int P(\alpha,\theta;R)\sin\theta\, d\theta\, R d\alpha\, dR=\int Q(r_1,r_2)dr_1dr_2\ .$$

In Eq. (8), though Ψ_{LM} is a function of four angular variables of two independent electrons, $\sum_M|\Psi_{\mathrm{LM}}|^2/(2L+1)$ is transformed to a function of only one angular variable θ by recoupling the single-electron angular momenta, and the integrals over the residual three angular variables result in the factor $8\pi^2$. The explicit form of ρ and the detailed explanation for its derivation are described in Ref. 9.

The states investigated here are the *nsns* states shown in Table I. For the 8*s*8*s* and 10*s*10*s* states, for each of which two energy levels are presented in Table I, we draw the plots for the one with $-0.079\,77$ a.u. and the one with $-0.046\,12$ a.u., respectively. The charge-density plots are shown in Figs. 4–10. In each figure, the uppermost drawing is an r_1-r_2 plot of the charge density, and the next one is its contour map. One or more α-θ plots of the charge density are shown below the contour map, and the hyperradius R at which each α-θ plot is drawn is indicated by an arc in the contour map. Note that the α-θ

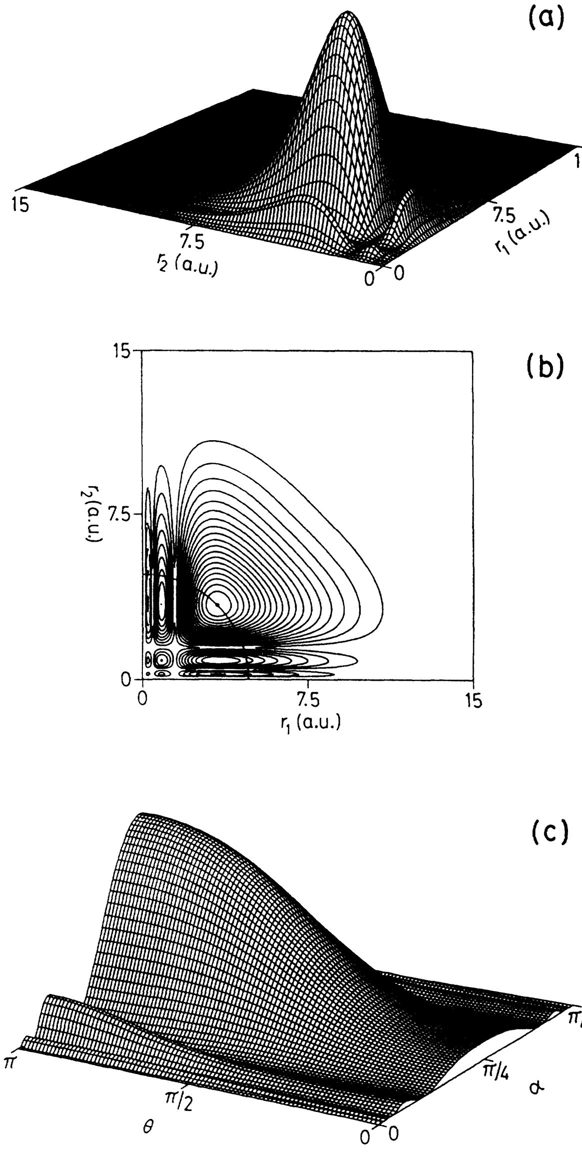

FIG. 4. Charge-density plots of the 4*s*4*s* state of Ca: (a) as a function of r_1 and r_2, (b) contour map of (a), and (c) as a function of the hyperspherical-coordinate variables α and θ with a fixed hyperradius ($R=4.8$ a.u.) equal to the radius of the arc drawn in (b).

plot is interpreted as a charge-density distribution obtained when the cross section along the arc is decomposed on θ.

In every r_1-r_2 plot, we can see a reasonably large part of the charge density to be localized at a location of the Wannier potential ridge,[8,20–22] that is, a large mountain lies at a place in which $r_1=r_2$, though many smaller peaks are dispersively distributed in the plots of higher states. The presence of this large mountain confirms that all the states presented here definitely possess a charac-

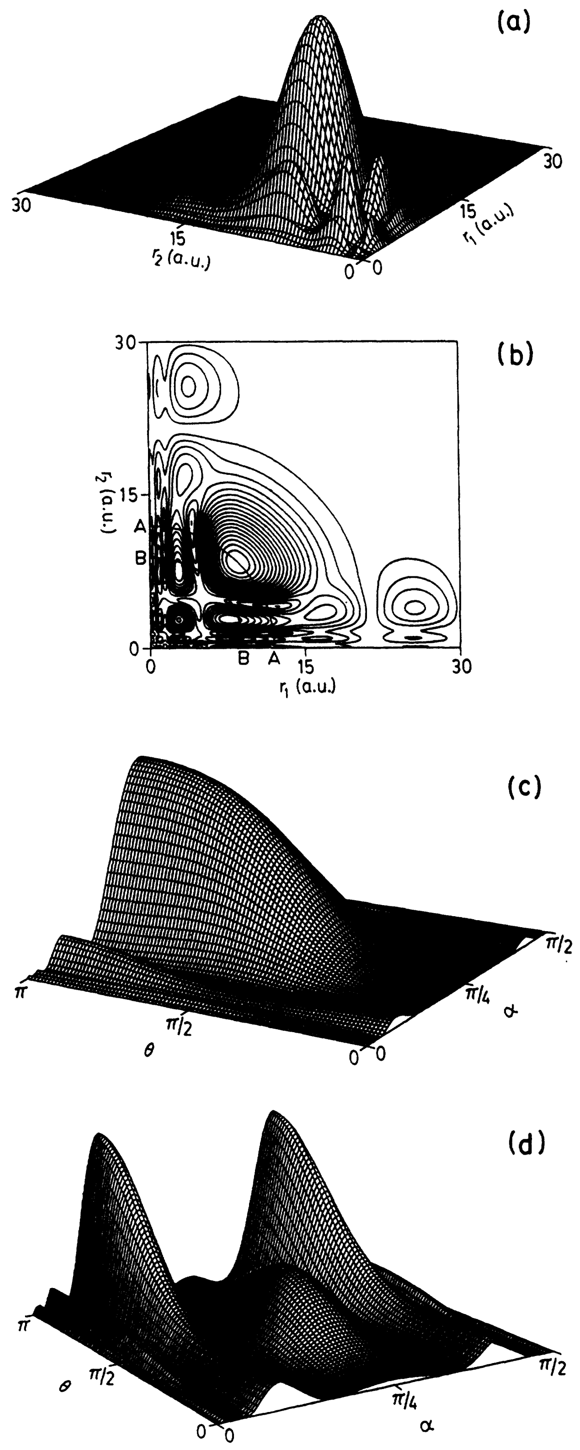

FIG. 5. Similar to Fig. 4 except for the 5s5s state: the plots as a function of α and θ are drawn with two differently fixed hyperradii, (c) $R=12.0$ a.u. and (d) $R=9.0$ a.u., equal to the radii of the arcs A and B in (b), respectively.

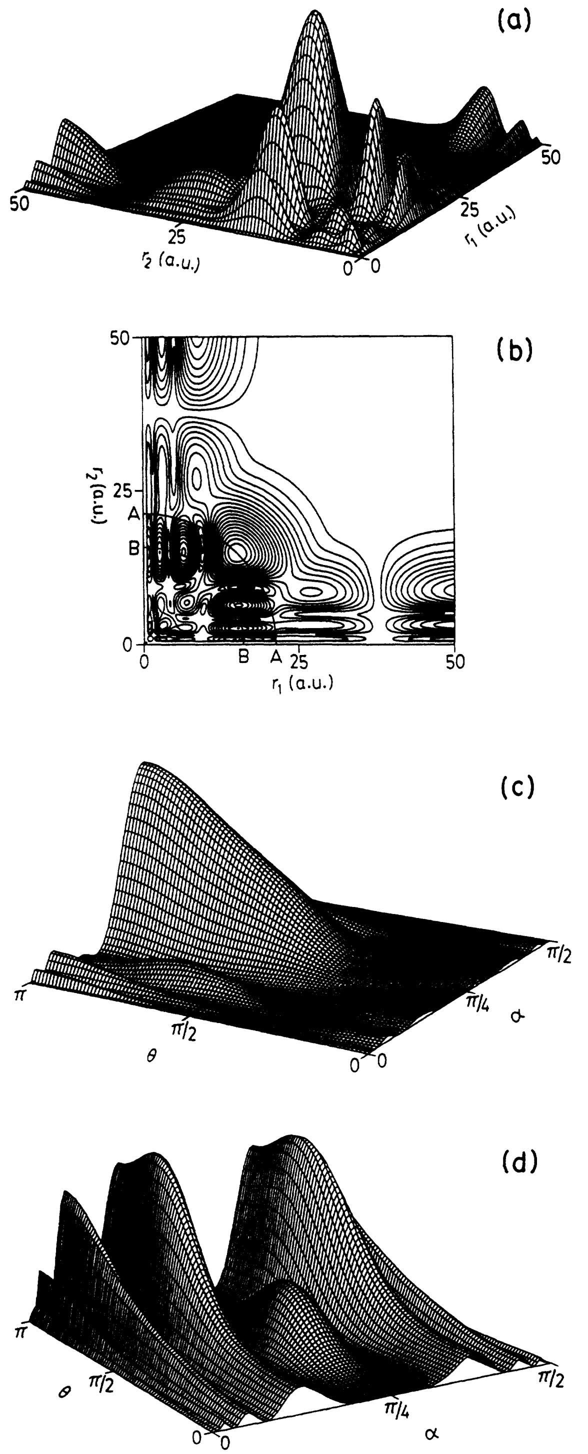

FIG. 6. Similar to Fig. 4 except for the 6s6s state: the plots as a function of α and θ are drawn with two differently fixed hyperradii, (c) $R=21.3$ a.u. and (d) $R=16.0$ a.u., equal to the radii of the arcs A and B in (b), respectively.

teristic of the Wannier-ridge-type state. Smaller peaks seen in the plots of higher states are mainly due to lower-lying Rydberg series. The presence of these peaks is unavoidable in the states higher than the $5s5s$ state, because one or more low-lying Rydberg series necessarily overlap in energy with those states. Because we are not interested in the components of the Rydberg states, our investigation is to be concentrated on the large mountain lying on the potential ridge. Thus, for each state, at least one α-θ plot is drawn with R fixed to the value at the peak of the mountain.

As seen in Fig. 4(c), the charge-density distribution in the α-θ plot of the $4s4s$ state is equivalent to that in the r_1-θ plot drawn by Krause and Berry,[14] and is similar to that of the $2s2s$ state of helium,[6,8,9] supporting the correctness of the moleculelike picture in the $4s4s$ state. It is clearly found by inspecting the eigenvector that this distribution is dominantly due to a simple $(4s4s+4p4p)$ configuration mixing.

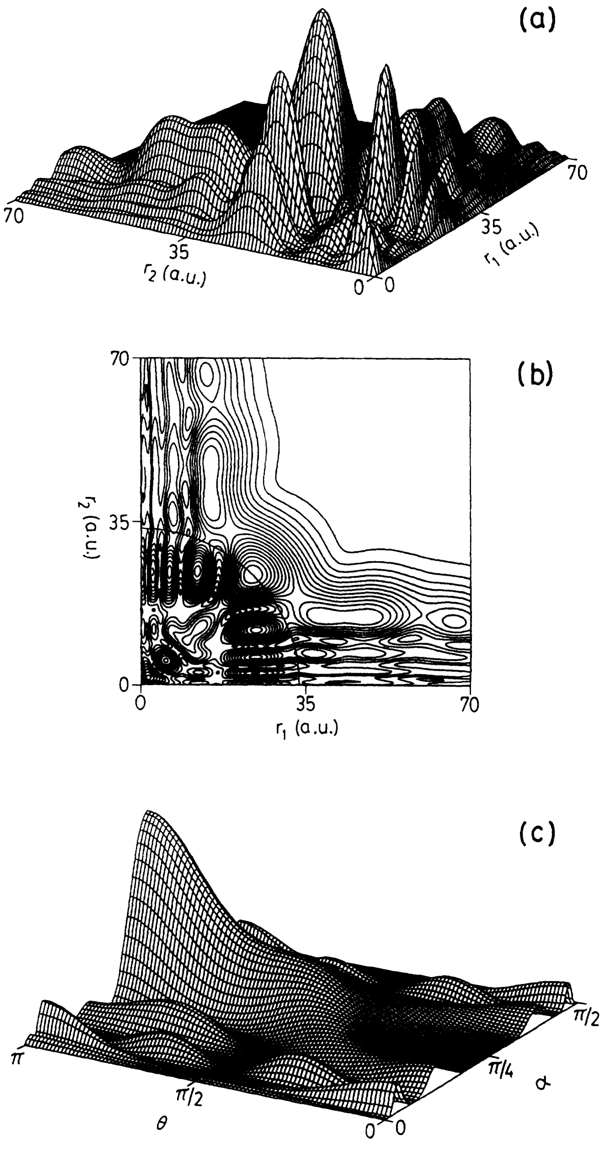

FIG. 7. Similar to Fig. 4 except for the $7s7s$ state: the plot (c) is drawn as a function of α and θ with a fixed hyperradius ($R=33.6$ a.u.) equal to the radius of the arc in (b).

In the $5s5s$ state, as seen in Fig. 5(c), the α-θ plot shows a charge-density distribution similar to that of the $4s4s$ state, though it is slightly more localized around $\theta=\pi$. This distribution is also likely to support the applicability of the moleculelike picture to the $5s5s$ state. As seen in Fig. 5(d), however, a characteristic, which is unusual in helium, begins to appear in this state; that is, the θ dependence at the inner foot of the mountain does not have a peak at $\theta=\pi$, but at $\theta=\pi/2$. This means that the two electrons' charge densities in a comparable distance from the core show a "bent" structure with respect to the core when the distance is smaller, while the densities show a normal linear-molecule-type structure when the distance is larger. It is found by inspecting the eigenvector that, in a viewpoint of configuration mixing, the peak around $\theta=\pi/2$ in Fig. 5(d) results from a contribution of the $4d4d$ base. In Ca^+, the $(n-1)d$ state is comparable to or slightly smaller than the ns and np states not only in energy but also in the radius at which their radial wave functions have the largest amplitude. Therefore, the $(n-1)d(n-1)d$ base is expected to play a role similar to the $ndnd$ base in helium. Although the $4d4d$ base indeed makes an appreciable contribution to the $5s5s$ state of Ca, the way of the contribution tends to be different from that in helium. In helium, the intrashell-type bases $(nlnl)$ mix with each other so as to sharpen the correlation peak at $\theta=\pi$. In fact, as shown in Fig. 11(b), the lowest ${}^1S^e$ state of $n=9$, which corresponds to the $9(8,0)^+9$ state in the notation developed by Lin,[6] shows an extremely sharp correlation at $\theta=\pi$. If we call this manner of mixing the *in-phase* manner, the $4d4d$ base of Ca is mixed in the *out-of-phase* manner with the fundamental $(5s5s+5p5p)$ configuration-mixed state. It is, in fact, found that the CI coefficient of the $4d4d$ base has a sign opposite to those of the $5s5s$ and $5p5p$ bases,[38] while in helium all the CI coefficients of the intrashell-type bases with a fixed n have a common sign. The effect of this out-of-phase mixing of the $4d4d$ base is not remarkable at the peak of the mountain, because the mountain is dominantly composed of the $5s5s$ and $5p5p$ bases and the CI coefficient of the $4d4d$ base is much smaller than those of the former bases. At the inner foot of the mountain, however, the effect of the $4d4d$ base becomes remarkable because of the slightly smaller radius at which the $4d$ radial wave function has the largest amplitude. Consequently, as is seen in Fig. 5(d), the $\theta=\pi$ correlation peak composed of the $5s5s$ and $5p5p$ bases is greatly lowered by the out-of-phase superposition of the $4d4d$ base and, instead, the $\theta=\pi/2$ peak peculiar to the $4d4d$ base becomes remakable.

This out-of-phase mixing of the $(n-1)d(n-1)d$ base is seen also in the eigenvector of the $4s4s$ state. In this case, however, the CI coefficient of the $3d3d$ base is too small for any apparent characteristic to appear in the charge-density plots. On the other hand, as shown in Fig. 6, the same feature as that described above for the $5s5s$ state is seen also in the $6s6s$ state, though the role of the $4d4d$ base is played by the $5d5d$ base in this case.

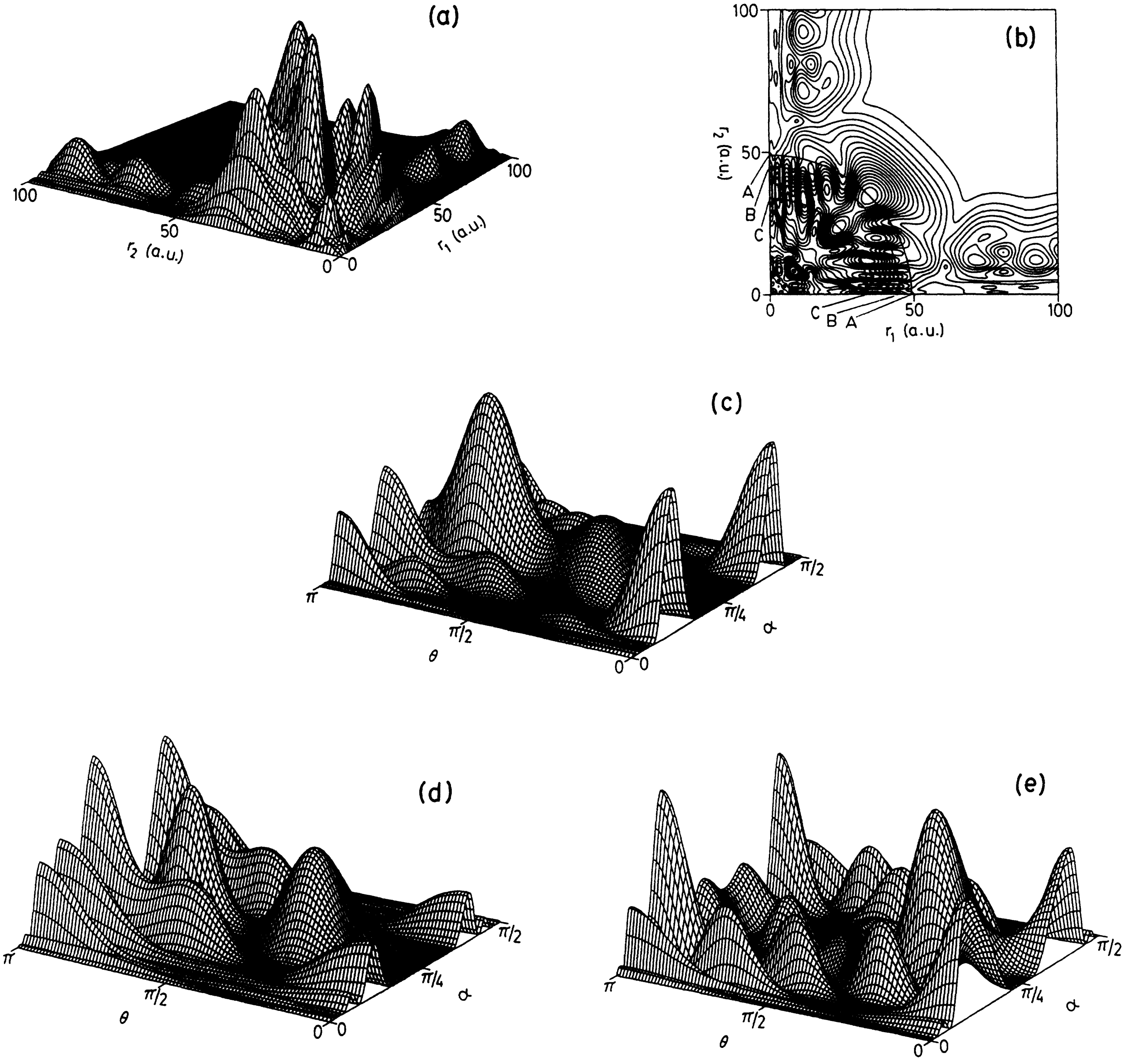

FIG. 8. Similar to Fig. 4 except for the $8s8s$ state: the plots as a function of α and θ are drawn with three differently fixed hyperradii, (c) $R = 49.1$ a.u., (d) $R = 45.0$ a.u., and (e) $R = 33.9$ a.u., equal to the radii of the arcs A, B, and C in (b), respectively.

The out-of-phase mixing causes much more remarkable effects on higher Wannier-ridge-type states. In those states, however, the $(n-2)l(n-2)l$ bases ($l \geq 3$) play important roles instead of the $(n-1)d(n-1)d$ base. Note that in Ca^+, similar to the $(n-1)d$ state, the $(n-2)l$ state ($l \geq 3$) is comparable to or slightly smaller than the ns and np states not only in energy but also in radius at which their radial wave functions have the largest amplitude. A typical example of the remarkable out-of-phase mixing is seen in the $8s8s$ state, as shown in Fig. 8. As mentioned before, the r_1-r_2 plots of higher states show more complicated correlation patterns because of lower-lying Rydberg series. In Fig. 8(a), we can see two highest peaks at the potential-ridge location. The outer one is mainly composed of the $8s8s$ and $8p8p$ bases, while the inner one is mainly due to a contribution of the $7sns$ Rydberg-type bases. Moreover, the $6g6g$ base considerably contributes to the composition of both peaks, while the $7d7d$ base no longer makes an appreciable contribution to any correlation pattern. Figure 8(c) shows the α-θ correlation along the arc passing through the outer highest peak of the r_1-r_2 plot. The θ dependence of the ridge component (which means the charge density along $\alpha = \pi/4$) in Fig. 8(c) shows a strange correlation, which is somewhat similar to that shown in Fig. 5(d) and does not have a peak at $\theta = \pi$, but has a large peak at $\theta = 0.78\pi$.

This correlation pattern is also likely to suggest a "bent" structure of the charge-density distribution. It is found by inspecting the eigenvector that this correlation pattern results from the out-of-phase mixing of the $6g6g$ base and is explained in the same manner as that described before concerning Fig. 5(d). In contrast with the case of the $5s5s$ state, the CI coefficient of the $6g6g$ base is so large that the highest peak, not the foot, of the mountain shows the bent structure.

The ridge component in Fig. 8(c) has also a small subpeak at $\theta=0.39\pi$, and this subpeak becomes more enlarged in Fig. 8(d), which shows the α-θ correlation along the arc passing slightly inside the outer highest peak in Fig. 8(a). This is because of a larger contribution from the $6g6g$ base at this radius than at the highest peak. This double-peak structure might be associated with a bending vibrational motion. The structure, however, is not what is attributed to the vibration, because it does not have a complete node but shows only a saddle-like form. At the inner highest peak, as seen in Fig. 8(e), the θ dependence of the ridge component becomes more wavy, and approaches a bare feature of the $6g6g$ base itself, though it is still deformed by other bases. This variation of the θ dependence with decreasing R shows that the $6g6g$ base plays a dominant role in the angular correlation of the ridge component.

A very similar α-θ correlation pattern is seen in the $10s10s$ state, as shown in Fig. 10(c). In this case, the out-of-phase mixing of the $8h8h$ and $8h9h$ bases dominantly causes the bent-type correlation pattern. It is also

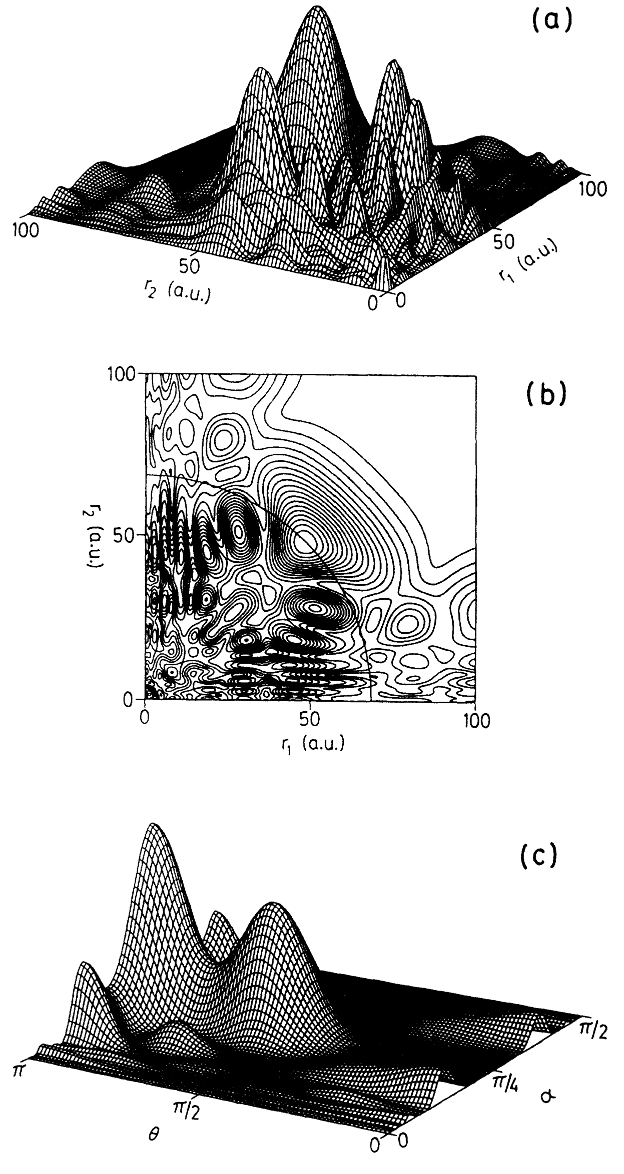

FIG. 9. Similar to Fig. 4 except for the $9s9s$ state: the plot (c) is drawn as a function of α and θ with a fixed hyperradius ($R=68.6$ a.u.) equal to the radius of the arc in (b).

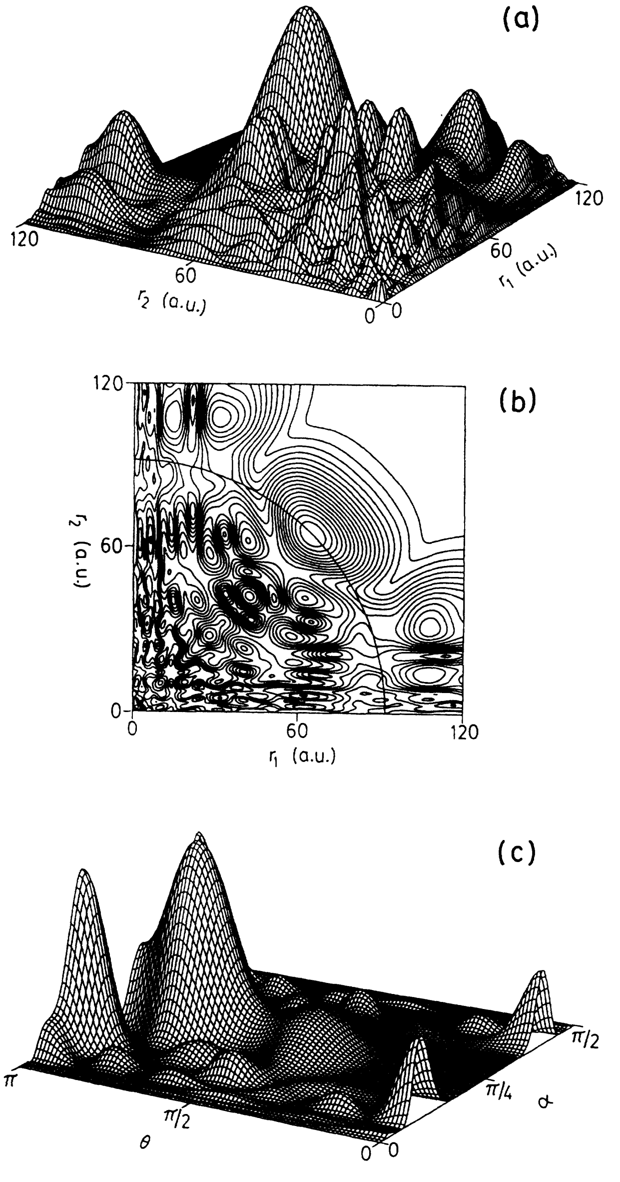

FIG. 10. Similar to Fig. 4 except for the $10s10s$ state: the plot (c) is drawn as a function of α and θ with a fixed hyperradius ($R=91.8$ a.u.) equal to the radius of the arc in (b).

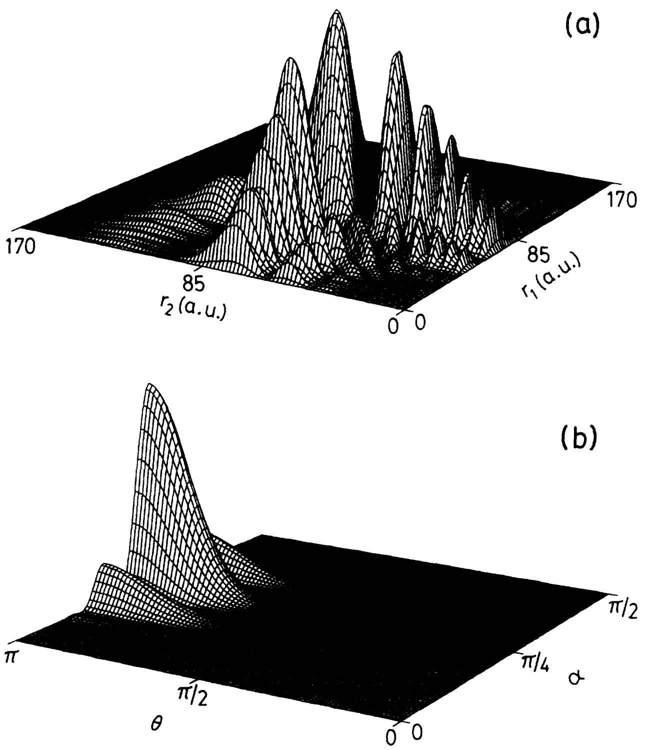

FIG. 11. Charge-density plots of the $9(8,0)^{+}9\ {}^1S^e$ state of He: (a) as a function of r_1 and r_2, and (b) as a function of the hyperspherical-coordinate variables α and θ with a fixed hyperradius $R=102.0$ a.u.

found by a detailed investigation that a variation of the angular correlation pattern at each smaller R is similar to that seen in the $8s8s$ state.

In contrast with the states investigated above, the in-phase mixing of the $(n-2)l(n-2)l$ bases ($l\geq 3$) is dominant in the $7s7s$ and $9s9s$ states. In Fig. 7(c) and Fig. 9(c), we can see a θ dependence quite different from that seen in the $8s8s$ and $10s10s$ states. In fact, the CI coefficients of the $7g7g$, $7h7h$, and $7i7i$ bases, which make a relatively large contribution to the $9s9s$ state, have the same sign as the $9s9s$ and $9p9p$ bases.[38] In the $7s7s$ state, though a contribution from the $(n-2)l(n-2)l$ bases ($l\geq 3$) is very small, the $5f6f$ and $5f7f$ bases, instead, appreciably contribute. Their CI coefficients also have the same sign as the $7s7s$ and $7p7p$ bases.[38] Note that, though the correlation pattern seen in Fig. 7(c) is somewhat similar to that in Fig. 6(c), the characteristic is essentially different; that is, in the $7s7s$ state, the θ dependence of the ridge component keeps to have its largest peak at $\theta=\pi$ even in the inner foot of the large mountain. This characteristic is also seen in the $9s9s$ state, and is peculiar to a correlation pattern resulting from the in-phase mixing.

Because of the in-phase mixing, the θ dependence of the ridge component in Fig. 9(c) is similar to that seen in a specific ${}^1S^e$ Wannier-ridge-state of helium; that is, the correlation pattern in Fig. 9(c) is similar to, for example, that shown in Fig. 12, in which the α-θ plot of the $9(6,0)^{+}9\ {}^1S^e$ state of helium is drawn. In the molecule-like picture, the latter state is interpreted as the lowest excited state of the bending-vibration mode with any rotation mode unexcited. In spite of the similarity, however, the correlation pattern seen in Fig. 9(c) is not attributed to the bending vibration. This is understood by the fact that the correlation pattern does not have a complete node but shows only a saddle-like form.

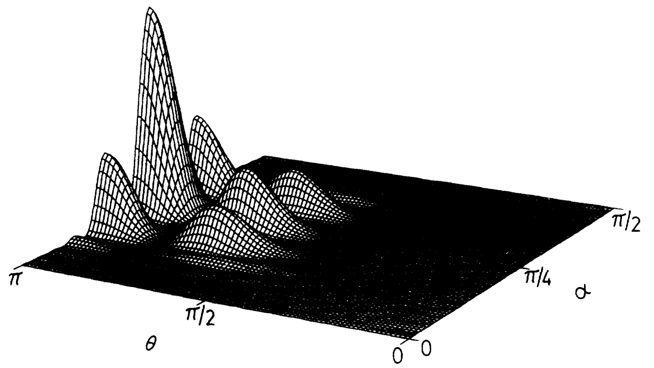

FIG. 12. Charge-density plot of the $9(6,0)^{+}9\ {}^1S^e$ state of He as a function of the hyperspherical-coordinate variables α and θ with a fixed hyperradius $R=96.9$ a.u.

As described above, in spite of the nondegeneracy in the Ca^{+} energy levels, higher Wannier-ridge-type states of calcium show a fairly strong angular correlation in their ridge components, although they do not necessarily show an extremely sharp correlation as seen in helium. The angular correlation patterns of Ca result from a rather simple configuration-mixing scheme. They are fundamentally dominated by the $(nsns+npnp)$ configuration mixing. This fact results in a less sharp pattern of the overall angular correlation. This fundamental pattern, having a broad peak at $\theta=\pi$, is then deformed by higher angular momentum bases, such as $(n-1)d(n-1)d$ and $(n-2)l(n-2)l$ for $l\geq 3$, forming unusual angular correlation patterns. There are two types of deformation; one is to sharpen the peak at $\theta=\pi$, as is similar to that in helium, and the other is to destroy the peak at $\theta=\pi$ and, instead, to form another peak at $\theta<\pi$. In the latter case, the resulting correlation pattern is suggestive of a bent structure of the charge-density distribution. It may be interesting that, in higher states, these two types of correlation patterns alternately appear with n increasing. With only the examples presented here, however, it is undeniable that this alternation is only accidental.

V. DISCUSSION

In Sec. IV we concentrated our interest only on the main ridge component (large mountain), because every state investigated has a well-defined ridge component, in which a reasonably large amount of charge density is localized. In higher states, however, a considerable amount of charge density is distributed also at the nonridge location. This distribution is mainly due to lower-lying Rydberg series. The strong mixing of the Rydberg states is, of course, because of the nondegeneracy in Ca^+ energy levels. Moreover, the manner of this mixing looks rather irregular, as seen in the r_1-r_2 plots. This irregularity presents a striking contrast to the beautiful correlation pattern of helium shown in Fig. 11(a). Considering this irregularity together with the unusual angular correlation of the ridge component, the applicability of the usual moleculelike picture to calcium is likely to be negative at least in higher states. Though the presence of an alternative collective motion is not necessarily impossible, it cannot be known from only the present results. To obtain information on this point, we need extensively investigate many states other than $^1S^e$. We would note that, in our preliminary calculation, some $^3P^o$ states show a bent-type correlation very similar to that seen in the $8s8s$ and $10s10s$ states. This fact might suggest the presence of a collective motion.

Whether or not a collective motion exists, however, the bent structure itself is interesting, because this structure means the breakdown of the axial symmetry of the charge-density distribution. A helium atom also shows a bent-type correlation pattern, which is attributed to a moleculelike state with the vibrational rotation excited. The bent structure of Ca, however, is seen in the $^1S^e$ state, which has no total angular momentum. Therefore, this bent structure cannot be attributed to the vibrational rotation. Instead, the bent structure might be attributed to the bending vibration. However, as seen in comparison with the pattern shown in Fig. 12, the bent-type correlation pattern of Ca is completely different from that attributed to the bending vibration in the usual moleculelike picture for helium. Thus, this bent-type correlation pattern is quite peculiar to calcium atoms or, probably, to alkaline-earth atoms.

An alternative structure[39] responsible for the bent-type correlation pattern is something like a "twisted bow tie" or a linear-type "propeller," which is also twisted between its wings. Also in this type of shape, a correlation function is expected to have a minimum at $\theta=\pi$ and a maximum at $\theta<\pi$, and the axial symmetry is broken. To obtain information on such a higher-order deformation, a higher-order angular correlation function must be investigated. It would be an interesting future work.

The essential configuration-mixing scheme causing this unusual correlation pattern is well understood, as detailed in the previous section. It is, however, still unknown what causes this manner of configuration mixing and what its physical meaning is. With only an analysis through a configuration-mixing scheme, it is difficult to gain a physical insight. Thus, the development of analytical treatments is strongly looked forward to.

ACKNOWLEDGMENTS

We would like to thank Dr. Masahiro Iwai for fruitful discussions throughout the present study and for his advice on calculation techniques. We would like to thank also Professor Hiroki Nakamura for his advice on the calculation technique in the early stage of the present work. Numerical calculations in the present study were carried out at the Computer Center of the Institute for Molecular Science, using a FORTRAN subroutine NSHOUD, written by Y. Beppu and I. Ninomiya, and using also DSCI3D and DSFI3D, written by K. Hatano. These subroutines are contained in Nagoya University Mathematical Program Package (NUMPAC) belonging to the above computer center.

---

*Present address: 1-chome 16-28, Higashi-chiyoda, Shizuoka, Japan.

[1] O. Sinanoglu and D. R. Herrick, J. Chem. Phys. **62**, 886 (1975); D. R. Herrick and O. Sinanoglu, Phys. Rev. A **11**, 97 (1975); M. E. Kellman and D. R. Herrick, J. Phys. B **11**, L755 (1978); D. R. Herrick and M. E. Kellman, Phys. Rev. A **21**, 418 (1980); D. R. Herrick, M. E. Kellman, and R. D. Poliak, *ibid.* **22**, 1517 (1980); M. E. Kellman and D. R. Herrick, *ibid.* **22**, 1536 (1980).

[2] D. R. Herrick, Adv. Chem. Phys. **52**, 1 (1982).

[3] C. E. Wulfman, Phys. Lett. **26A**, 397 (1968); C. E. Wulfman, in *Group Theory and Its Applications,* edited by E. M. Loebel (Academic, New York, 1971), Vol. 2; Chem. Phys. Lett. **23**, 370 (1973).

[4] J. W. Cooper, U. Fano, and F. Prats, Phys. Rev. Lett. **10**, 518 (1963).

[5] J. Macek, J. Phys. B **1**, 831 (1968).

[6] C. D. Lin, Phys. Rev. A **25**, 76 (1982); **26**, 2305 (1982); **27**, 22 (1983); **29**, 1019 (1984); C. D. Lin and J. H. Macek, *ibid.* **29**, 2317 (1984); S. Watanabe and C. D. Lin, *ibid.* **34**, 823 (1986).

[7] N. Koyama, H. Fukuda, T. Motoyama, and M. Matsuzawa, J. Phys. B **19**, L331 (1986); H. Fukuda, N. Koyama, and M. Matsuzawa, *ibid.* **20**, 2959 (1987); T. Motoyama, N. Koyama, and M. Matsuzawa, Phys. Rev. A **38**, 670 (1988).

[8] See for a review U. Fano, Rep. Prog. Phys. **46**, 97 (1983); U. Fano and A. R. P. Rau, *Atomic Collisions and Spectra* (Academic, Orlando, 1986).

[9] G. S. Ezra and R. S. Berry, Phys. Rev. A **25**, 1513 (1982); **28**, 1974 (1983); **28**, 1989 (1983).

[10] G. H. Wannier, Phys. Rev. **90**, 817 (1953).

[11] M. Iwai, J. Phys. Soc. Jpn. **57**, 2225 (1988); M. Iwai and H. Nakamura, Phys. Rev. A **40**, 2247 (1989).

[12] C. H. Greene, Phys. Rev. A **23**, 661 (1981).

[13] P. F. O'Mahony and C. H. Greene, Phys. Rev. A **31**, 250 (1985); P. F. O'Mahony, *ibid.* **32**, 908 (1985); P. F. O'Mahony and S. Watanabe, J. Phys. B **18**, L239 (1985).

[14] J. L. Krause and R. S. Berry, Phys. Rev. A **31**, 3502 (1985); J. Chem. Phys. **83**, 5153 (1985).

[15] K. Bartschat, M. R. H. Rudge, and P. Scott, J. Phys. B **19**, 2469 (1986).

[16] M. Aymar, E. Luc-Koenig, and S. Watanabe, J. Phys. B **20**, 4325 (1987); M. Aymar, *ibid.* **20**, 6507 (1987); M. Aymar and J. M. Lecomte, *ibid.* **22**, 223 (1989).

[17] M. Aymar, Phys. Rep. **110**, 163 (1984).

[18] C. H. Greene and L. Kim, Phys. Rev. A **36**, 2706 (1987); L. Kim and C. H. Greene, *ibid.* **36**, 4272 (1987).

[19] L. Kim and C. H. Greene, Phys. Rev. A **38**, 2361 (1988).

[20] F. H. Read, J. Phys. B **10**, 449 (1977); S. J. Buckman, P. Hammond, F. H. Read, and G. C. King, *ibid.* **16**, 4219 (1983).

[21] A. R. P. Rau, J. Phys. B **16**, L699 (1983).

[22] C. D. Lin and S. Watanabe, Phys. Rev. A **35**, 4499 (1987).

[23] W. E. Cooke, T. F. Gallagher, S. A. Edelstein, and R. M. Hill, Phys. Rev. Lett. **40**, 178 (1978).

[24] S. A. Bhafti, C. L. Cromer, and W. E. Cooke, Phys. Rev. A **24**, 161 (1981).

[25] N. H. Tran, R. Kachru, and T. F. Gallagher, Phys. Rev. A **26**, 3016 (1982); N. H. Tran, P. Pillet, R. Kachru, and T. F. Gallagher, *ibid.* **29**, 2640 (1984).

[26] R. M. Jopson, R. R. Freeman, W. E. Cooke, and J. Bokor, Phys. Rev. Lett. **51**, 1640 (1983).

[27] L. A. Bloomfield, R. R. Freeman, W. E. Cooke, and J. Bokor, Phys. Rev. Lett. **53**, 2234 (1984).

[28] P. Camus, P. Pillet, and J. Boulmer, J. Phys. B **18**, L481 (1984).

[29] J. Boulmer, P. Camus, and P. Pillet, J. Opt. Soc. Am. B **4**, 805 (1987); P. Camus, T. F. Gallagher, J.-M. Lecomte, P. Pillet, L. Pruvost, and J. Boulmer, Phys. Rev. Lett. **62**, 2365 (1989).

[30] T. F. Gallagher, J. Opt. Soc. Am. B **4**, 794 (1987).

[31] N. Morita, T. Suzuki, and K. Sato, Phys. Rev. A **38**, 551 (1988).

[32] N. Morita and T. Suzuki, J. Phys. B **21**, L439 (1988).

[33] W. E. Cooke and C. L. Cromer, Phys. Rev. A **32**, 2725 (1985).

[34] M. J. Seaton, Rep. Prog. Phys. **46**, 167 (1983).

[35] A. R. P. Rau, J. Opt. Soc. Am. B **4**, 784 (1987).

[36] M. Aymar, J. Phys. B **22**, 2359 (1989).

[37] H.-T. Wang, J. Phys. B **19**, 3401 (1986).

[38] At least for $^1S^e$ states, the angular part of $\sum_M |\Psi_{\rm LM}|^2$ in Eq. (8) always has a positive sign at $\theta = \pi$. The sign of the radial wave function of each single-electron state is chosen so that its largest peak is positive. Therefore, whether the correlation peak at $\theta = \pi$ in the $\alpha - \theta$ plot is increased depends on whether each CI coefficient of the bases has a common sign.

[39] Suggested by M. Iwai (private communication).